Seamlessly Converged Fiber-Wireless Access Networks with Dynamic Sub-wavelength Switching and Tunable Photonic mmWave Generation

Vallejo Castro, Luis; Gonem, Omaro; Jin, Wei; Giddings, Roger; Chen, Lin; Huang, Yi; Yi, Xingwen; Faruk, Md Saifuddin; Tang, Jianming

Journal of Lightwave Technology

Peer reviewed version

[Cyswllt i'r cyhoeddiad / Link to publication](#)

Seamlessly Converged Fiber-Wireless Access Networks with Dynamic Sub-wavelength Switching and Tunable Photonic mmWave Generation

Luis Vallejo, *Member, IEEE*, Omaro Fawzi Abdelhamid Gonem, *Student Member, IEEE*, Wei Jin, *Member, IEEE*, Roger Philip Giddings, Lin Chen, Yi Huang, Xingwen Yi, Md Saifuddin Faruk, and Jianming Tang.

Abstract—For implementing next-generation radio access networks (NG-RANs) supporting services/applications in the beyond-5G (B5G) era, seamless fiber-wireless network convergence is vital for enabling heterogeneous signals of various characteristics to continuously flow between the optical and electrical domains, i.e., the baseband unit (BBU) and user equipment (UE), without optical-electrical-optical (O-E-O) conversions or digital signal processing (DSP) at any intermediate nodes. To address such challenges, this paper proposes and experimentally demonstrates, for the first time, a cost-effective fiber-wireless converged flexible and dynamic access network based on intensity modulation and direct detection (IM-DD). The demonstrated network utilizes O-E-O conversion-free Soft-reconfigurable optical add/drop multiplexers (Soft-ROADMs) at remote nodes to dynamically establish connections between the BBU and the remote radio heads (RRHs) at the sub-wavelength level. In addition, free-running laser-enabled photonic millimeter-wave (mmWave) signal generation and passive electrical envelope detector-enabled mmWave down-conversion are also used, respectively, at the RRHs and UEs to achieve mmWave frequency tunability and adaptive wireless network coverage. The network performance and optimum network configuration are experimentally explored extensively in a fiber-wireless converged access network with 3×1.333 Gbps dynamic BBU-UE connections over a 10 km IM-DD fiber link and a 5 m, 38 GHz mmWave wireless link. The results show that wide mmWave frequency tuning ranges and adaptive mmWave coverages are achievable by just adjusting the RRH-laser frequency and output powers.

Index Terms—B5G, sub-wavelength-level all-optical switching, fiber-wireless converged access network, reconfigurable optical add/drop multiplexer (ROADM), millimeter-wave (mmWave), free-running laser, envelope detector.

I. Introduction

THE global mobile traffic is forecasted to exceed 465 exabytes (EB) per month by 2030, with >17.1 billion mobile subscribers and >97 billion machine-to-machine (M2M) subscriptions [1, 2]. Beyond-Fifth-generation (B5G) mobile access networks are required to deliver unprecedented peak data rates of ≥ 1 Tbit/s, ultra-low latencies of $10 - 100$ µs, and massive connection densities of 10 million devices/km^2 [3]. In addition, the dynamic nature of mobile traffic and diverse requirements of emerging services in terms of bandwidth and latency also impose significant technical challenges for practically implementing next-generation radio access networks (NG-RANs) capable of cost-effectively delivering these B5G key performance indicators (KPIs) [4].

To address the aforementioned technical challenges, the adoption of millimeter-wave (mmWave) wireless communications, already introduced in 5G new radio (NR) [5, 6], is essential for boosting the capabilities of NG-RANs [7, 8]. Additionally, it is also highly desirable to seamlessly converge different fiber and wireless network segments to enable heterogeneous signals of various characteristics (modulation formats, bandwidth, etc.) to continuously flow across the entire access network between the baseband unit (BBU) and the user equipment (UE), without requiring either optical-electrical-optical (O-E-O) conversions or extensive digital signal processing (DSP) at any intermediate nodes. However, achieving such seamlessly converged fiber-wireless access

L. Vallejo, O. F. A. Gonem, W. Jin, R. P. Giddings, X. Yi, M. S. Faruk, J. Tang are with the DSP Centre of Excellence, School of Computer Science and Engineering, Bangor University, Dean Street, LL57 1UT, Bangor, United Kingdom. (e-mail: l.vallejocastro@bangor.ac.uk; o.gonem@bangor.ac.uk; w.jin@bangor.ac.uk; r.p.giddings@bangor.ac.uk; x.yi@bangor.ac.uk; m.faruk@bangor.ac.uk; j.tang@bangor.ac.uk).

L. Chen is with College of Electronics and Information Engineering, Shanghai University of Electric Power, 200090, Shanghai, China. (email: chenlin1008@shiep.edu.cn).

Y. Huang is with Key Laboratory of Specialty Fiber Optics and Optical Access Networks, Shanghai University, 200444, Shanghai, China. (email: huangyi1008@shu.edu.cn).

networks fully supporting mmWave communications not only necessitates the deployment of cost-effective DSP-free mmWave signal generation/detection techniques at the remote radio heads (RRHs), but also requires the NG-RANs to be equipped with O-E-O conversion-free and DSP-free switching devices, which can be used in the intermediate nodes between the BBU and the RRHs for achieving dynamic BBU-RRH signal routing with fine optical granularity.

Several DSP-free mmWave signal generation techniques have been reported. Because commercially available electrical devices often have limited bandwidths, those techniques using electrical local oscillators (LOs) and RF mixers for electrical mmWave up/down-conversions are relatively expensive for practically implementing NG-RANs featuring excellent mmWave frequency tunability within an ultra-wide frequency range [9, 10, 11, 12]. Whilst photonics-aided techniques based on optical beating between two optical wavelengths in a photodetector (PD), where the generated mmWave frequency equals the frequency difference between these two involved optical signals, are relatively simple and cost-effective for achieving the aforementioned desirable NG-RANs, due to optical components' wide bandwidth, existing lasers' excellent wavelength tunability and ultra-wide tuning range, as well as continuously developed/matured photonic integration [9, 11, 12, 13]. As a direct result, several photonics-aided techniques have been demonstrated to act as high-quality mmWave sources, such as laser phase locking [14, 15, 16], and dual-wavelength lasers [17]. Furthermore, external modulators can also be used to generate two optical sidebands with a frequency gap equal to a specific mmWave frequency [18, 19]. Moreover, optical non-linear effects such as four-wave mixing (FWM) and stimulated Brillouin scattering (SBS) [20, 21] can also be incorporated into the above external modulator-based techniques for achieving large mmWave frequencies.

In comparison with all of the above photonics-aided mmWave generation techniques, the use of two independent lasers acting as two beating optical signals, here known as the free-running laser technique, is highly desirable due to their simplicity and cost-effectiveness [9]. For practical implementations, one laser resides in the BBU and is modulated for optical data transmission, and the other laser can be located at the RRH to produce the mmWave signal via RRH-PD-based optical beating. In comparison with hosting both lasers at the BBU, apart from improving the network spectral utilization efficiency, such implementation also ensures that: i) the RRH-laser outputs do not suffer fiber transmission-induced power loss; ii) the requirements of using extra optical amplifiers to boost the two signal powers launched into the RRH-PD for producing mmWave signals with required specific powers are relaxed; and iii) the requirements of the high-gain electrical amplifiers (EAs) for boosting the generated mmWave signal are also relaxed. However, for the free-running laser-based mmWave generation approach, the generated mmWave signal suffers the relatively strong effects of phase noise and frequency fluctuation due to the beating of two independent optical sources. To address this issue, on the UE side, passive electrical envelope detectors (EDs) can be used to achieve simple and cost-effective mmWave signal down-conversion, which is significantly less sensitive to mmWave carrier phase noise and frequency fluctuation [22, 23, 11, 24].

As one of the widely used optical switching devices, O-E-O conversion-free reconfigurable optical add/drop multiplexers (ROADMs) [25, 26] play a key role in achieving the aforementioned seamless fiber-wireless access network convergence for providing fast and dynamic BBU-RRH traffic routing [27, 28, 29]. Several O-E-O conversion-free ROADMs have been reported for the NG-RANs. However, the existing techniques mainly relying on Mach-Zehnder interferometers (MZIs) [30, 31] and Micro-ring resonators (MRRs) [32] can only provide wavelength-level optical switching and are unable to cost-effectively deal with dynamic mobile traffic with flexible and fine granularity. To address such technical challenges, Soft-ROADMs [33, 34] capable of offering both wavelength-level and sub-wavelength-level optical switching are highly desirable. The Soft-ROADM wavelength-level and sub-wavelength-level add operations are achievable using widely commercially available passive optical couplers (OCs) [33]. For dropping a targeted RF signal conveyed by an individual wavelength without O-E-O conversions, here termed sub-wavelength-level drop operation, the Soft-ROADM utilizes an optical intensity modulator, driven by a sinusoidal drop RF signal, to optically shift the targeted signal band to an unoccupied baseband spectral region [33, 35]. Furthermore, the Soft-ROADM can also offer wavelength-level drop operation by simply setting the optical intensity modulator as an "on/off" optical switch [33, 36]. The Soft-ROADM wavelength-level and sub-wavelength-level drop operations have excellent transparency to input signal characteristics (modulation format, bitrate, bandwidth, and signal band RF location and wavelength) [33, 34].

To cost-effectively deliver the aforementioned seamless fiber-wireless network convergence for the NG-RANs, this paper proposes and experimentally demonstrates, for the first time to the authors' knowledge, a novel fiber-wireless converged flexible and dynamic intensity modulation and direct detection (IM-DD) access network, by employing O-E-O conversion-free Soft-ROADMs and free-running laser-(electrical ED)-enabled mmWave signal generation (detection). The Soft-ROADMs are used at the intermediate nodes, named remote nodes (RNs) between the BBU and the RRHs, to support agile, dense, and "just-the-right-size" BBU-RRH connectivity at both wavelength and sub-wavelength levels. Each RRH is equipped with an independent laser with its wavelength dynamically tuned to produce the mmWave signal at the desired frequency by optical beating between the RRH-laser optical signal and the Soft-ROADM-dropped signal without any optical filtering. Passive electrical EDs are also used at the UEs to enable an electrical LO-free direct down-conversion of the received mmWave signals, thus giving rise to excellent transparency to mmWave frequency.

To provide comprehensive comparisons between the proposed network and the existing fiber-wireless converged access network solutions with dynamic BBU-RRH traffic routing, Table I is presented where the comparisons are made

TABLE I

QUALITATIVE COMPARISONS OF FIBER-WIRELESS CONVERGED ACCESS NETWORKS WITH DYNAMIC BBU-RRH TRAFFIC ROUTING

Ref.	Optical Steering, mmWave Generation and Detection	Architecture and Complexity	Latency (**L**), Scalability (**S**), wireless Frequency Tunning Flexibility (**FT**), transmission performance/network coverage adaptability (**Ad**)
[37]*	• Time-division-multiplexing (TDM)-based optical switching. • Mixing electrical LO and intermediate frequency (IF) /mmWave signals for mmWave up/down-conversion.	• Central Control Unit transmits separate wavelengths respectively conveying low-frequency LOs and IF signals to Radio Access Units (relatively high fiber transmission losses). • Radio Access Units use electrical frequency multipliers for up-converting low-frequency LO signals to required mmWave frequencies. • mmWave sources are used at terminal user ends. • Low bandwidth PDs, high-speed TDM optical switches.	• **L**: low, no O-E-O conversions/DSP at intermediate nodes, constrained by optical switching speed and TDM delay. • **S**: constrained by utilized optical switch port count and switching capability. • **FT**: constrained by electrical LO tunability and electrical frequency multipliers. • **Ad**: n. a.
[38] [39] [40]	• Arrayed waveguide grating router (AWGR) (wavelength-level routing, suitable for TDM/WDM scenarios). • Mixing electrical LO and signals for mmWave up/down-conversion.	• Central Unit uses multiple tunable lasers each having dynamic wavelength tunability to modulate user data (at different time slots) on different wavelengths for achieving wavelength-level routing at AWGR-based remote nodes. • AWGR (4 dB insertion loss) and low bandwidth PDs. • Electrical LO for mmWave up/down-conversion.	• **L**: low, no O-E-O conversions/DSP at intermediate nodes, constrained by laser tuning speed and TDM delay. • **S**: constrained by laser count and AWGR input/output port. • **FT**: constrained by electrical LO tunability. • **Ad**: n. a.
[30] [31] [41] [42] [43]	• Cascaded (Mach–Zehnder interferometer) MZI-based ROADM (wavelength-level add/drop). • Mixing electrical LO and IF signals for mmWave up/down-conversion.	• Electrical LO for mmWave up/down-conversion. • MZI-based optical filters are used for wavelength-level drop operations. • 2.5 dB (5 dB) power loss for supporting 2 (4) wavelengths (resulting from Si_3N_4 ROADMs). • Low bandwidth PDs.	• **L**: low, no O-E-O conversions/DSP at intermediate nodes, constrained by ROADM configuration latency. • **S**: constrained by ROADM input/output port numbers. • **FT**: constrained by electrical LO tunability. • **Ad**: n. a.
[29] [32] [44]	• Micro-ring resonators (MRR)-based optical switch (wavelength level switching). • Mixing electrical LO and IF signals for wireless signal up/down-conversion.	• Electrical LO for wireless signal up/down-conversion. • MRR add-drop filters are used, as multiplexers/demultiplexers, for performing wavelength-level switching. • 15 dB~20 dB switching operation loss due to fiber coupling and on-chip losses. • Optical amplifiers. Low bandwidth PDs.	• **L**: relatively low, no O-E-O conversions/DSP at switching nodes, constrained by optical switch configuration latency and RRH DSP. • **S**: constrained by optical switch input/output port numbers. • **FT**: constrained by electrical LO tunability. • **Ad**: n. a.
This work	• Soft-ROADM with sub-wavelength and wavelength-level add/drop operations. • Optical beating of the soft-ROADM dropped signal (baseband) and RRH-embedded free-running laser optical signal at the RRH-PD for mmWave generation. • ED-based mmWave detection at UEs without electrical LOs and mixers.	• A free-running tunable laser with a high output power is used at each RRH for mmWave generation and upstream transmissions, thus relaxing the requirement of high BBU launch powers (potentially increasing network adaptability to support multiple wavelengths). • Soft-ROADM power losses depend on ROADM architectures and intensity modulators employed for realizing drop operations. For MZM-based intensity modulators, the drop elements have a power loss of 5 dB~8 dB. • Simple mmWave generation and detection due to the exclusion of electrical LO, mixer, and frequency multipliers at both RRHs and UEs. • High bandwidth PDs.	• **L**: low, no O-E-O conversions/DSP at intermediate nodes, constrained by drop RF signal generation/updating speed. • **S**: theoretically unlimited, because of its inherent adaptability to wavelength count variations and each wavelength capable of supporting ultra-dense and customizable BBU-UE connections. Wavelength count constrained by practical Soft-ROADM architectures. • **FT**: easily achievable by simply adjusting RRH-laser wavelength. The tuning range is proportional to PD bandwidth. • **Ad**: easily achievable by simply controlling RRH-laser output power adaptively.

Note: *: WDM-based routing is not evaluated in the reference and thus is not considered in the table.
        n.a.: not available from references.

in terms of major technical aspects including optical steering method, mmWave generation/detection, network architecture, complexity, latency, scalability, and frequency tuning flexibility, as well as network coverage adaptability. From Table I, it can be found that with neither extensive DSP nor O-E-O conversions at any intermediate nodes, the proposed network not only enables seamless signal flows between BBUs and UEs across the fiber and wireless network segments, but also possesses excellent new features including: i) agile, ultra-dense and customizable BBU-UE connection provisions according to actual service requirements; ii) Soft-ROADM-enabled flexible and dynamic switching at both wavelength and sub-wavelength levels; iii) a wide mmWave frequency tunning range by simply adjusting RRH-laser wavelengths; iv) adaptable wireless coverages by simply changing RRH-laser optical powers; and v) simplified ED-induced mmWave down-conversion in UEs.

The performances of the proposed access network are experimentally explored in a fiber-wireless converged access network with 3×1.333 Gbps flexible BBU-UE connections established over a 10 km IM-DD optical link and a 5 m at 38 GHz mmWave wireless link. The optimum network configuration is also identified for not only improving the transmission performance but also lowering the overall network power consumption and expenditure.
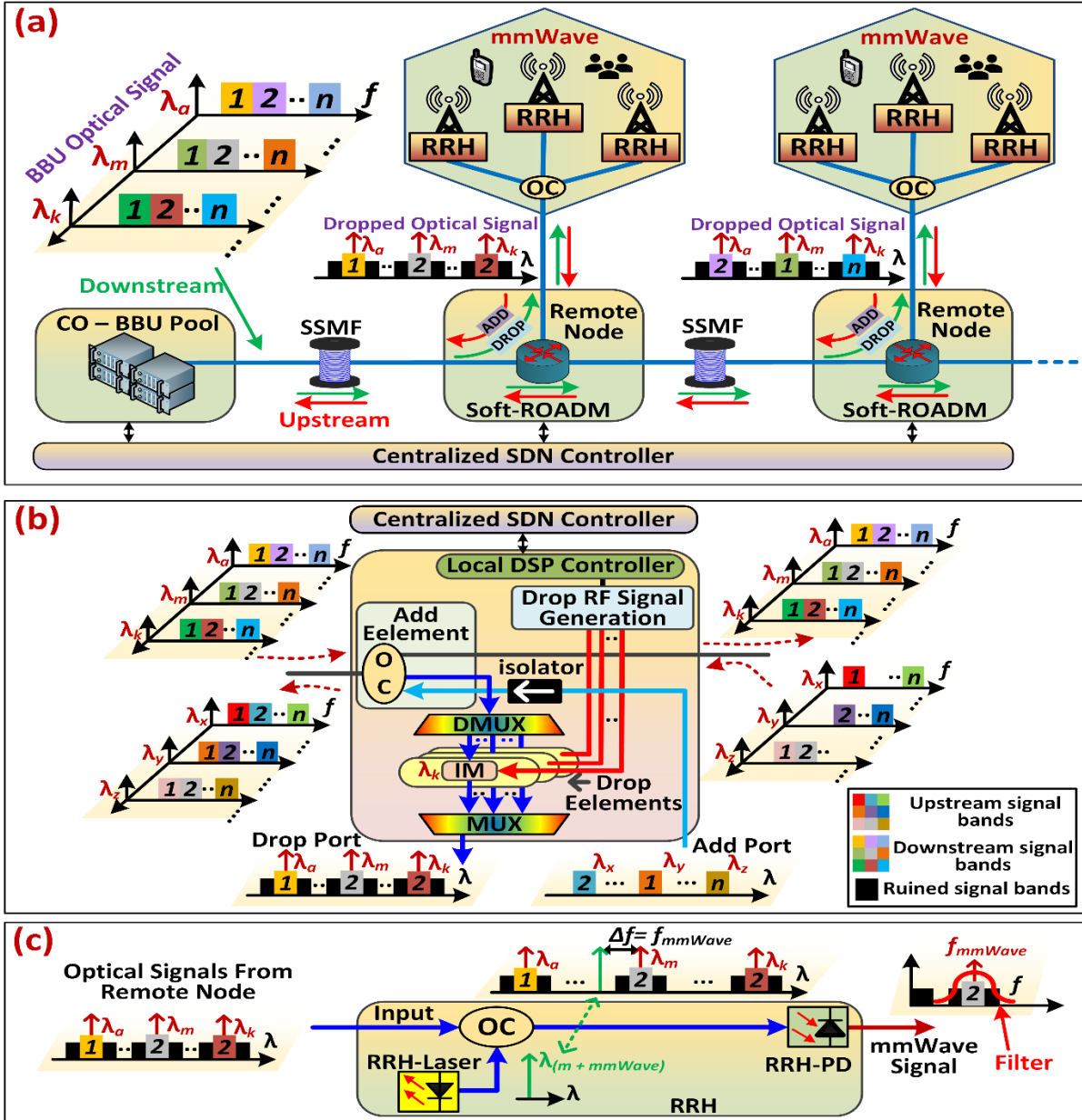
Fig. 1 (a) SDN-controllable fiber-wireless converged dynamic and flexible IM-DD access networks employing O-E-O conversion-free Soft-ROADMs and free-running laser-(electrical ED)-enabled mmWave signal generation (detection), (b) Soft-ROADM architecture, (c) wavelength selection and optical beating for mmWave signal generation at RRHs. IM: intensity modulator, MUX: wavelength multiplexer, DMUX: wavelength demultiplexer, OC: optical coupler.

II. FIBER-WIRELESS CONVERGED DYNAMIC AND FLEXIBLE IM-DD ACCESS NETWORKS

A. Operating Principle

Fig. 1(a) illustrates the proposed fiber-wireless converged access network capable of dynamically and flexibly establishing, via software-defined networking (SDN), fast and ultra-dense connections between the BBU and all UEs without implementing O-E-O conversions and DSP at any intermediate nodes. An O-E-O conversion-free SDN-controllable Soft-ROADM [33, 34, 36] is employed at each RN to implement dynamic optical switching at wavelength and sub-wavelength levels. Cost-effective SDN-controllable free-running laser-

(electrical ED)-enabled mmWave signal generation (detection) can be employed for cost-effectively producing (down-converting) the mmWave signals at the desirable frequencies.

In the central office (CO), as seen in Fig. 1(a), multiple wavelengths, each containing multiple gapless signal bands at different RFs, termed sub-wavelengths, are produced by intensity modulation. Each signal band corresponds to an independent channel. The bandwidth and signal modulation format can be adaptively adjusted for each channel individually via SDN to meet the requirements of a specific BBU-UE communication service.

For a specific wavelength, the CO-produced optical signal containing u independent signal bands can be expressed as [35]:

$$E_{CO}(t) = \sqrt{1 + m\sum_{i=1}^{u} a_i(t)\,cos(2\pi f_i t)} \qquad (1)$$

where $a_i(t)$ is the i-th signal, which is up-converted to the RF of f_i. m is the intensity modulation index. Conventional up-conversion techniques or digital filter multiplexing (DFM) techniques [45] can be employed to generate these multiple signal bands practically. It is worth mentioning that for each wavelength, the baseband spectral region of the CO-produced optical signal can (not) be occupied if the wavelength (sub-wavelength) drop operation is implemented at the corresponding RN.

In each RN, as seen in Fig. 1(b), the embedded Soft-ROADM passively splits the received optical signals into three copies. One copy is delivered to the next RN. For the remaining copy, the wavelengths are passively separated by a wavelength demultiplexer (DMUX), and each wavelength is then directed into an independent Soft-ROADM drop element.

For implementing the sub-wavelength level drop operation, in each drop element, a sinusoidal RF signal, labeled drop RF signal, which is produced locally under the control of SDN, is employed to drive an intensity modulator [33]. The drop RF signal frequency equals the central frequency of the targeted signal band. To drop a targeted signal, $a_c(t)$, the employed drop RF signal, with an amplitude of A_c, can be written as:

$$S_{RF-c}(t) = A_c\,cos(2\pi f_c t) \qquad (2)$$

When the transmission systems are assumed to be ideal and lossless, after the Soft-ROADM sub-wavelength drop operation, the output of the Soft-ROADM drop element can be expressed as [33, 34, 35]:

$$E_{drop}(t) = \sqrt{1 + \frac{mm_1 A_c}{2} a_c(t) + Q(t)} \qquad (3)$$

where m_1 is the modulation index adopted in the Soft-ROADM drop operation. $a_c(t)$ is the targeted signal, which is shifted to the unoccupied baseband spectral region. $Q(t)$ is the parasitic component containing all other unwanted signal bands which are fully destroyed and located at the high RFs, which can be expressed as:

$$\begin{aligned}
Q(t) &= \frac{mm_1 A_c}{2} a_c(t)\,cos(4\pi f_c t) + m_1 A_c\,cos(2\pi f_c t) \\
&\quad + m\sum_{i=1}^{u} a_i(t)\,cos(2\pi f_i t) \\
&\quad + \left[mm_1 A_c\,cos(2\pi f_c t)\left(\sum_{i=1,i\neq c}^{u} a_i(t)\,cos(2\pi f_i t) \right) \right]
\end{aligned}$$
$$\qquad (4)$$

To achieve the optimum sub-wavelength-level drop operation, large intensity modulation indexes should be used in the Soft-ROADM drop elements [36]. Such sub-wavelength-

level drop operations are transparent to input signal characteristics including, for example, modulation format, bitrate, bandwidth, and signal band RF location as well as wavelength. All the dropped optical signals are then combined using a wavelength multiplexer (MUX) and transmitted and broadcast to the corresponding RRHs.

At each RRH, as seen in Fig. 1(c), to convert the targeted signal of a specific wavelength (λ_m) to a mmWave signal at a frequency of f_{mmWave}, the RRH-laser output wavelength ($\lambda_{m+mmWave}$) is tuned to have a frequency gap (Δf) equal to the desirable mmWave frequency (f_{mmWave}) with respect to the targeted signal wavelength (λ_m). The desired mmWave signal is then produced by optical beating between the RRH-laser output signal and the received optical signals (the Soft-ROADM-dropped signals) from the RN. Due to the sub-wavelength-level drop operation, the targeted signal is at the central frequency of the produced mmWave signal. After high pass filtering to remove the undesirable parasitic components arising from the optical beating of the unwanted wavelengths, the mmWave signal is then transmitted to the corresponding UEs.

It is worth mentioning that, after the optical beating, if the produced mmWave signal band and the above-mentioned parasitic components are not spectrally overlapped, no extra optical filters are required to be used before the RRH-PD for extracting the targeted signal band wavelength. This can be achieved by adopting sufficiently large wavelength spacings between every two adjacent wavelengths. A 200 GHz wavelength-division multiplexing (WDM) grid would be sufficient to support a frequency detuning range from 24 GHz to 71 GHz, as required by the 3rd Generation Partnership Project (3GPP) [6].

At each UE, a passive electrical ED is used to directly down-convert the received mmWave signal to the baseband spectral region, which, due to the sub-wavelength-level Soft-ROADM drop operation, allows the UE receiver to use a low-speed analog-to-digital converter (ADC), operating only at the bandwidth of the targeted signal band without the need to cover all signal bands, as verified in Section III. The UE DSP employs conventional signal demodulation procedures. More importantly, such a mmWave down-conversion has excellent transparency to mmWave frequency, thereby equipping the proposed technique with excellent mmWave frequency tunability, as verified by Section IV.B.

Apart from the sub-wavelength-level drop operation, the Soft-ROADMs can also offer wavelength-level optical switching. No drop RF signals are required, and the Soft-ROADM-embedded intensity modulators act as "off-state" optical switches, which prevent the unwanted wavelengths from being sent to the RRHs. In addition, the Soft-ROADM can also be configured as an "on-state" optical switch (optical passway) to enable the corresponding entire wavelengths to be dropped and sent to the RRHs [36].

For upstream transmissions, the Soft-ROADMs use passive optical couplers to realize wavelength-level and sub-wavelength-level add operations. The achievable add operation performances have been thoroughly investigated in both offline [46, 47] and real-time [33] experiments. This work mainly

focuses on the sub-wavelength-level drop operations for the downstream transmissions.

From the above analyses, it is easy to understand that the proposed network potentially possesses excellent wavelength selectivity, because: i) the Soft-ROADM drop elements can act as "off-state" optical switches to prevent the routing of unwanted wavelengths to a RRH, thus offering a Soft-ROADM-enabled wavelength selection, and ii) each RRH can dynamically change the wavelength of its embedded tunable laser to ensure that it is close to the desirable wavelength to produce a desirable mmWave signal.

B. Optimum Network Configuration

For the proposed network, the produced mmWave signal frequency and power can be adaptively changed to meet various application requirements in terms of network/cell deployment, transmission performance, and mmWave coverage. The flexible mmWave signal frequency variation can be achieved by just adjusting the RRH-embedded laser output wavelength, as verified by Section IV.B.

Reducing/increasing the produced mmWave signal power can be achieved by i) decreasing/increasing the RRH-laser output power; and ii) decreasing/increasing the RRH-received optical signal power. The experimental results in Section IV.C indicate that for dynamically altering the produced mmWave signal powers, adjusting the RRH-embedded laser output power is more efficient than adjusting the RRH-received optical signal power via optical amplifier gain control.

III. EXPERIMENTAL SETUP

Fig. 2 shows the experimental setup of the proposed fiber-wireless converged dynamic and flexible IM-DD access network with sub-wavelength-level Soft-ROADM drop operation and free-running laser-(electrical ED)-based mmWave signal generation (detection). A single wavelength transmission case is considered here as a proof-of-concept.

In the CO-BBU transmitter, an arbitrary waveform generator (AWG) operates at $f_{DAC} = 32$ GS/s @8-bit and produces a 0.7 V_{pp} electrical analog signal. As shown in inset (i) of Fig. 2, the produced signal contains three independent 2 GHz-bandwidth RF orthogonal frequency division multiplexing (OFDM) bands centered at 3 GHz, 5 GHz, and 7 GHz, respectively. Each signal band has a bit rate of 1.333 Gbps, which gives rise to a total bit rate of 4 Gbps.

The conventional DFM approach [45] is used to produce these RF OFDM bands in the digital domain. First, three independent real-valued baseband OFDM signals are produced. Each signal contains six 16-quadrature amplitude modulation (QAM)-encoded data-carrying subcarriers by adopting the Hermitian symmetry at the input of a 32-point inverse fast Fourier transform (IFFT) operation. The OFDM cyclic prefix is 12.5%. Each resultant baseband OFDM signal is then digitally up-sampled by a factor of M = 8, before being digitally filtered to locate the signal at the desired RF spectral region. The three adopted digital filters are produced by cosine modulation of a standard baseband square root raised cosine (SRRC) filter [48]. The central frequencies of the three digital filters are set to be

$[2q - 1] \times f_{DAC}/2M$, where $q = 2, 3, 4$, respectively. The SRRC filter has zero excess bandwidth and a filter length of 32. After digital filtering, the produced RF OFDM bands are digitally combined and then oversampled by a factor of 2 to constrain the signal bandwidth to be within $2 - 8$ GHz. The baseband frequency region of $0 - 2$ GHz is kept free for the sub-wavelength-level drop operation, as illustrated in inset (i) of Fig. 2.

A 35 GHz-bandwidth integrated optical transmitter is employed to perform the electrical-to-optical (E-O) conversion at the CO-BBU. The optical transmitter consists of an internal EA, a tunable laser-1 (TL), and a quadrature-biased Mach-Zehnder modulator-1 (MZM) with an automatic bias controller (ABC). The TL-1 generates a 13.5 dBm optical carrier at 1550.516 nm. The bias voltage of MZM-1 is -1.5 V. The AWG-produced electrical signal with a 0.7 V_{pp} amplitude is amplified by a 19 dB EA, resulting in a ~17 dBm MZM driving signal. The optical power launched into the standard single-mode fiber (SSMF) is fixed at $P_{CO} = 0$ dBm.

After 10 km SSMF transmissions, at the RN, an erbium-doped fiber amplifier (EDFA) is employed to boost and fix the optical signal power to 10 dBm at the EDFA output, followed by a 1 nm tunable optical band-pass filter (OBPF) to remove out-of-band noise. In the Soft-ROADM drop element, a 50 GHz quadrature-biased MZM, driven by a sinusoidal drop RF signal, is employed to drop the targeted OFDM band without O-E-O conversions or DSP. A polarization controller (PC) is utilized to adjust the MZM input optical signal's polarization state. The drop RF signal, with an amplitude of 0.25 V_{pp}, is generated by a LO, and its frequency is adjusted to 3 GHz, 5 GHz, and 7 GHz for dropping the OFDM band-1, band-2, and band-3, respectively. A variable phase shifter (PS) followed by a 33 dB-gain EA-1 and a variable electrical attenuator-1 (VEA) are employed to optimize the drop RF signal phase and power. To achieve the optimum sub-wavelength level drop operation for the considered experimental setup, VEA-1 is adjusted to offer an extra 1.5 dB attenuation apart from its insertion loss of ~2 dB. After the drop operation, the targeted OFDM band is shifted to the free baseband region with a bandwidth of 1 GHz. The optical signal power at the output of the Soft-ROADM drop element (P_{Signal}) is 0.65 dBm.

It is worth mentioning that to achieve the optimum drop operation, the phases of the drop RF signal and the targeted signal should be matched. In the experiment, the phase of the drop RF signal is adjusted to match the phase of the targeted signal band using a variable PS. When a phase offset occurs, the power of the targeted signal band after the drop operation is reduced. The inset (ii) of Fig. 2 presents the RN-received optical signal spectra before the drop operation, which is measured by an optical spectrum analyzer (OSA) with 0.8 pm (100 MHz) resolution bandwidth (RBW). Whereas, The insets (iii) and (iv) of Fig. 2 illustrate the optical signal spectra after the drop operation (measured at the Soft-ROADM MZM output) with and without the drop RF signal phase offset. Detailed discussions on the impact of the drop RF signal phase offset can be found in [35, 49]. For practical implementations, a dual-arm
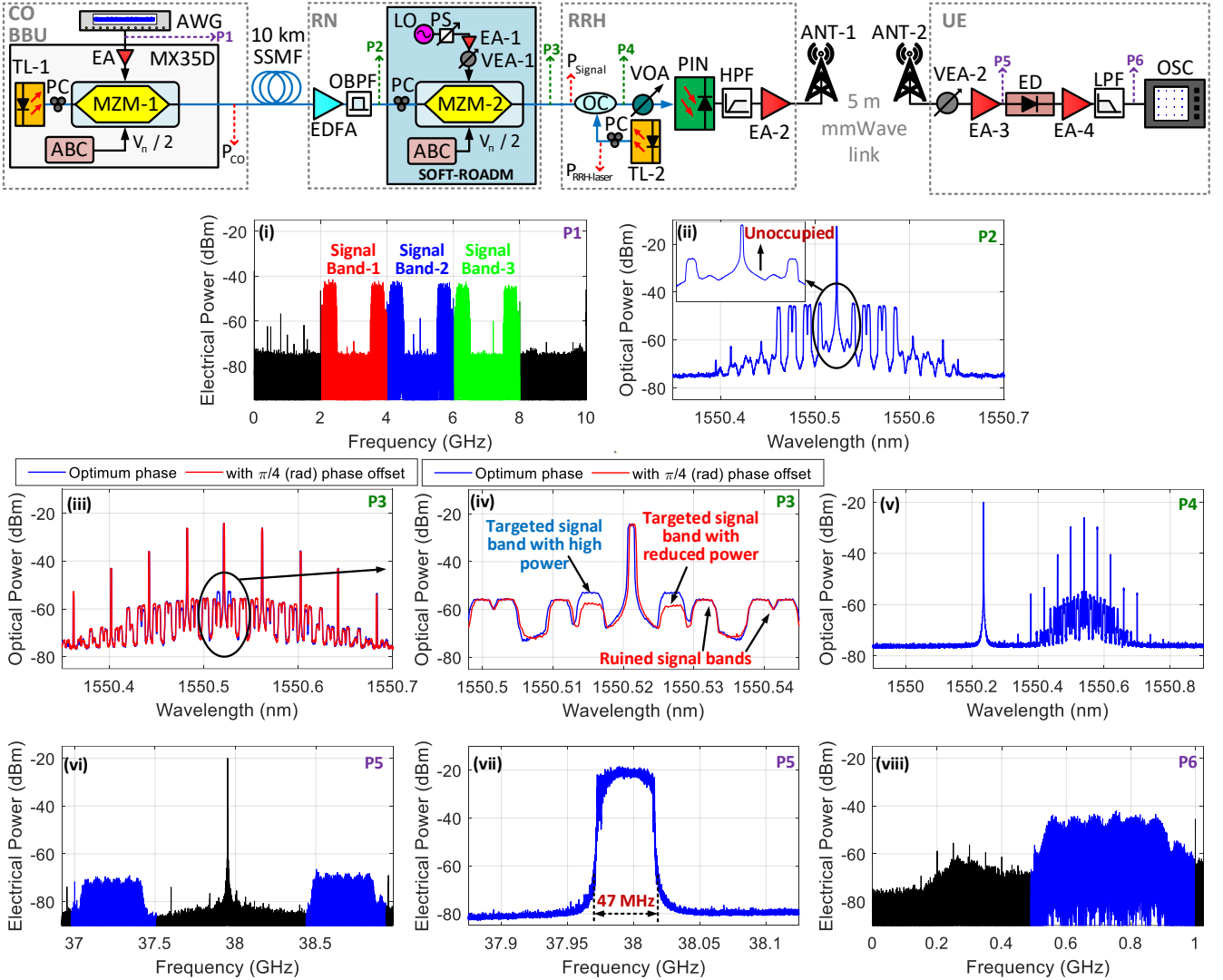
Fig. 2 Experimental setup of fiber-wireless converged dynamic and flexible IM-DD access networks with sub-wavelength-level Soft-ROADM drop operations and free-running laser-(electrical ED)-enabled mmWave generation (detection). Insets show the electrical (RBW = 10 kHz) and optical spectra (RBW = 0.8 pm) at different points. Inset (i): electrical signal spectra of the CO-BBU data signal, inset (ii): optical signal spectra at the input of the Soft-ROADM drop element, insets (iii) and (iv): optical signal spectra at the output of the Soft-ROADM drop element, inset (v): optical signal spectra before beating in RRH-PD, inset (vi): electrical signal spectra of the generated mmWave signal, inset (vii): measured mmWave carrier frequency fluctuation over 15-minute durations, inset (viii): electrical signal spectra of the baseband signal after envelope detection.

IQ Soft-ROADM drop element [35, 49] may be used to provide phase-offset-insensitive drop operation.

At the RRH, for producing mmWave signals at 38 GHz, a standalone TL-2 with an optical power ($P_{RRH\text{-}laser}$) of 2.5 dBm at 1550.213 nm is employed. The Soft-ROADM-dropped optical signal and TL-2 output optical signal are passively combined by a 50:50 OC, and the inset (v) of Fig. 2 illustrates the resultant optical signal spectrum. A variable optical attenuator (VOA) then adjusts the total received optical power (RoP) of the PIN-type PD. The PD has a 40 GHz bandwidth and a 0.7 A/W responsivity. After the PD, the generated mmWave signal, with the targeted OFDM band centered at 38 GHz, passes through a 26 – 50 GHz high-pass filter (HPF) before being amplified by a 28 dB-gain EA-2. The two horn antennas-1/2 (ANT) operate at 26.5 – 40 GHz and have a gain of 25 dBi.

After 5 m wireless transmissions, at the UE, the received mmWave signal power is dynamically adjusted by a VEA-2

followed by a 30 dB-gain EA-3. VEA-2 introduces a 5 dB power attenuation and a ~5.6 dB insertion loss. The resulting mmWave spectrum is illustrated in inset (vi) of Fig. 2. The received mmWave signal is then directly down-converted to the baseband region by a passive 33 – 50 GHz ED. After that, the resulting signal is amplified by a 22 dB-gain EA-4 and filtered using a 1.3 GHz-bandwidth low-pass filter (LPF). The spectrum of the baseband signal at the output of the LPF is presented in inset (viii) of Fig. 2. Finally, the electrical baseband signal is digitized, using an oscilloscope (OSC) operating at 4 GS/s, and is then processed offline for data recovery using conventional OFDM demodulation procedures.

It is important to highlight that the sub-wavelength-level drop operations of the Soft-ROADM allow the UE to operate at the dropped OFDM signal bandwidth (2 GS/s). However, in this setup, an OSC sampling speed of 4 GS/s is chosen to reduce the aliasing effects due to the non-ideal frequency response of the

UE-employed LPF. A digital-domain 2× down-sampling operation is thus performed after 1 GHz digital low-pass filtering and synchronization operations.

In addition, the BBU and RRH lasers (TL-1 and TL-2) are free-running external cavity lasers with 10 kHz linewidths. The inset (vii) of Fig. 2 presents the measured mmWave carrier frequency fluctuations over a 15-minute duration. The measurements are conducted by repeatedly and continuously measuring the carrier frequency and the maximum amplitude of the received mmWave carrier at the UE side before envelope detection. The observed mmWave carrier frequency fluctuation is ~47 MHz. However, due to the ED-enabled phase-offset/frequency-fluctuation-insensitive direct mmWave down-conversion, no extra DSP is required at the UE for mitigating the effects of phase noise and frequency fluctuation.

IV. RESULTS AND DISCUSSION

A. Transmission Performances

Using the experimental setup and parameters described in Section III, the measured bit error rate (BER) versus RoP performances for the three involved OFDM bands are illustrated in Fig. 3. The RoP denotes the total optical power launched into the PD for generating the mmWave signals at the RRH.

In this figure, three cases are considered. Case-1 is the "optical back-to-back (oB2B) link" case, where both fiber and wireless links are excluded, and ANTs and EA-2 are not used. After the HPF, the generated mmWave signal is directly delivered to the receiver, where the ED is employed for signal down-conversion before conventional signal demodulation. Case-2 is the "10 km SSMF link" case. This case adopts an experimental setup similar to Case-1, apart from passing the optical signals over a 10 km SSMF. The wireless link, ANTs and EA-2 are excluded. Case-3 is the "10 km SSMF + 5 m mmWave wireless link" case, presented in Fig. 2 and already explained in detail in Section III.

The results in Fig. 3 show that for all the considered cases, similar BER performances are observed for the low-frequency OFDM band-1 and band-2. For Case-3, in comparison with the two low-frequency OFDM bands, the high-frequency OFDM band-3 suffers ~1 dB degradations in the receiver sensitivity, defined as the minimum RoP for achieving BERs of $3.8×10^{-3}$ at

the considered 7% overhead hard-decision forward error correction (HD-FEC) limit [50, 51]. This is mainly due to the transmission system frequency response differences between these signal bands. To mitigate these performance variations across different RF bands, adaptive bit-loading and/or power-loading techniques may be employed. In addition, the fiber link-induced receiver sensitivity degradations are < 0.4 dB, and the mmWave link-induced receiver sensitivity degradations are < 1 dB.

Overall, the performance similarity of the considered OFDM bands indicates that the proposed network can use different RFs within each individual wavelength to simultaneously establish multiple connections between the BBU and various UEs at different locations. Because all the considered OFDM bands present similar performances, only OFDM band-2 performances are presented in the following sections for simplicity.

B. mmWave Frequency Tunability

Using the experimental setup explained in Section III, to evaluate the mmWave frequency tunability of the proposed network, the RRH-embedded TL-2 laser wavelength is flexibly adjusted to generate the desired mmWave frequency by optical beating without reconfiguring all other electrical/optical components.

Fig. 4(a) shows the BER performance of OFDM band-2 after 10 km SSMF and 5 m mmWave wireless transmissions. 35 GHz, 38 GHz, and 41 GHz mmWave carrier frequencies are considered. The results show that, the 38 GHz and 35 GHz mmWave transmissions have similar performances. However, when increasing the mmWave frequency to 41 GHz, ~3.3 dB receiver sensitivity degradations are observed mainly due to the bandwidth limitation of the RRH-employed 40 GHz PD.

Fig. 4(b) further evaluates the mmWave frequency tunability for different RoPs. Within the considered mmWave frequency tuning range from 35 GHz to 41 GHz, for each RoP, the BER performances of the OFDM band-2 are measured after 10 km SSMF and 5 m mmWave wireless transmissions. The results show that increasing the RoP can effectively and flexibly broaden the achievable mmWave frequency tuning range. For RoPs ≥ -1 dBm, the proposed network achieves a > ± 3 GHz dynamic mmWave frequency tuning range with respect to 38 GHz. It is worth highlighting that a slight BER degradation is
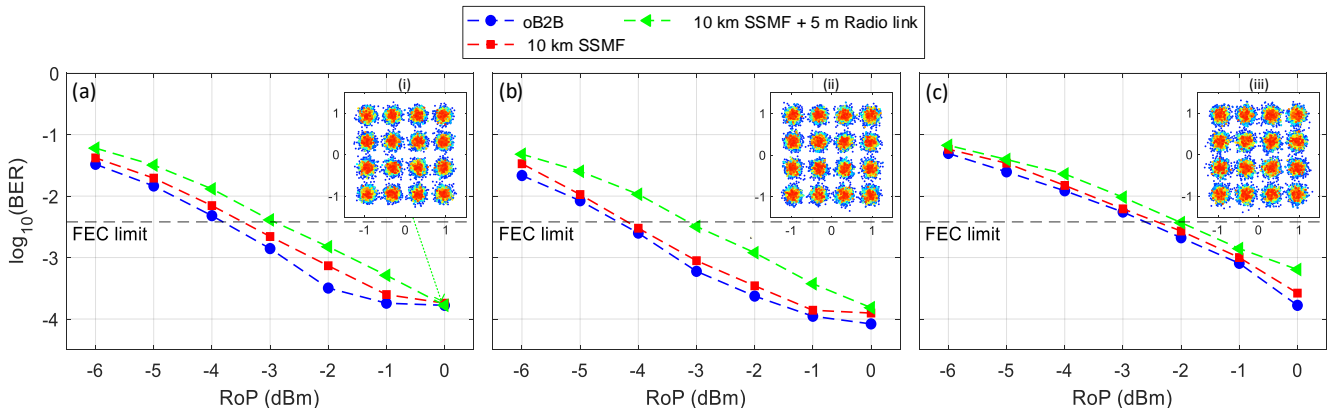

Fig. 3. BER performances of (a) OFDM band-1, (b) OFDM band-2, and (c) OFDM band-3. Insets show the observed constellations at a RoP of 0 dBm.
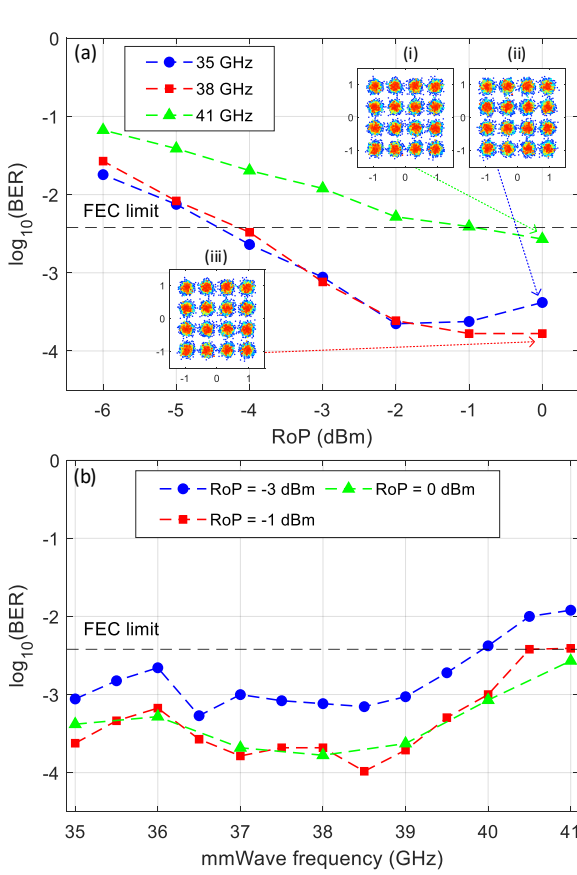
Fig. 5. mmWave frequency tunability. (a) OFDM band-2 BER versus RoP performance for different mmWave frequencies, and (b) OFDM band-2 BER performance versus mmWave frequency for different RoPs. Insets in (a) show the observed constellations at a RoP of 0 dBm.
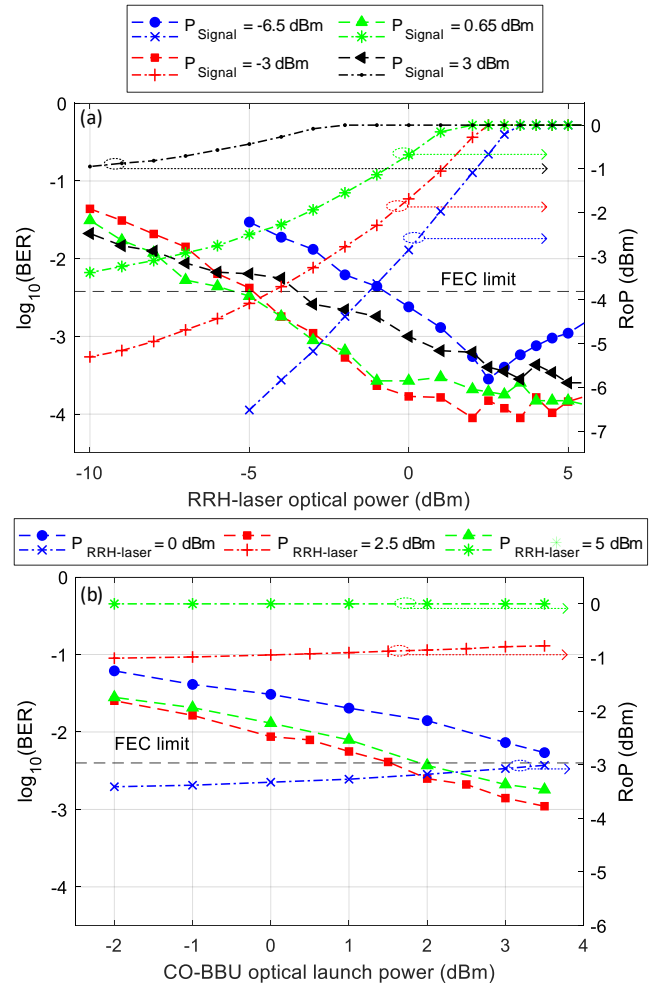

Fig. 4. OFDM band-2 BER performance for (a) different RRH-laser output powers and different RRH-received optical signal powers, and (b) CO-BBU optical signal launch powers and different RRH-laser output powers. In obtaining (b), all EDFAs and OBPFs are excluded in the experimental setups. Dash-dotted lines present corresponding RoPs. (dashed line: BER (left y-axis), dash-dotted line: RoP (right y-axis)).

observed at 36 GHz, mainly due to the frequency response characteristics of the electrical components, including ED, HPF, and EAs. Furthermore, as mentioned above, the bandwidth limitations of the employed RRH-PD also result in performance degradations for mmWave frequencies above 40 GHz.

Overall, the results in Fig. 4 imply that for the proposed network, via just controlling each RRH's laser wavelength, dynamic and flexible mmWave frequency tuning can be obtained for each cell. This may increase the cell capacity or effectively reduce the radio interference between adjacent cells. It should be highlighted that the mmWave tunability range can be wider when RRH-PDs with higher bandwidths are utilized.

C. mmWave Signal Power Optimisation

As mentioned in Section II.B, for the proposed network, the RRH-produced mmWave signal powers can be adjusted by altering the RRH-received optical signal powers and the RRH-embedded laser output powers. It is, therefore, vital to identify the optimum network configuration to produce the mmWave signals with desirable powers for achieving specific transmission performances and/or wireless network coverages.

Utilizing the experimental setup and parameters described in Section III, the impacts of the RRH-embedded laser output power ($P_{RRH-laser}$) and the RRH-received optical signal power (P_{signal}) on the BER performance of OFDM band-2 are

illustrated in Fig. 5(a). Different RRH-received optical signal powers are achieved by adjusting the EDFA output powers. At the RRH, due to the PD's maximum input optical power limitation, the VOA used before the PD restricts the RoPs ≤ 0 dBm.

As seen in Fig. 5(a), for each considered RRH-received optical signal power, increasing the RRH-laser output power from -10 dBm to 2 dBm can improve the transmission performances due to the increase in the produced mmWave signal powers. However, a further increase in the RRH-laser output power beyond that region cannot lead to considerable performance improvements. This is because, as seen in Fig. 5(a), the RoP, plotted on the right y-axis, reaches and remains at 0 dBm, thus limiting the power enhancement of the produced mmWave signal. Furthermore, Fig. 5(a) implies that increasing the RRH-received optical signal power from -6.5 dBm to -3 dBm improves the transmission performances because of the increased mmWave signal powers. However, a further increase in the RRH-received optical signal powers cannot lead to noticeable performance improvements. Increasing the RRH-received optical signal power (P_{signal}) from 0.65 dBm to 3 dBm

even degrades the performance, as a large EDFA gain reduces the optical signal-to-noise ratio (OSNR) of the RRH-received optical signal. The results imply that for altering/enhancing the produced mmWave signal powers, altering/increasing the RRH-laser output power is more efficient than altering/increasing the RRH-received optical signal powers via optical amplifier gain adjustment.

On the other hand, high RRH-laser output powers can effectively reduce the number of EDFAs and OBPFs required to establish the BBU-RRH links, thus reducing the overall network operational expenditures. This is verified by Fig. 5(b), where the OFDM band-2 BERs can still be below the FEC limit after removing all the EDFAs and OBPFs between the BBU and the RRH in the experimental setups. Due to the exclusion of EDFAs, the RRH-received optical signal power is controlled by adjusting the BBU-output optical signal power. As expected, a relatively high BBU-output optical signal power results in a relatively high RRH-received optical signal power, thus leading to improved transmission performances. Under such a network configuration, increasing the RRH-laser output power also effectively improves the transmission performance. However, such performance improvements would be weakened when the resulting RoPs exceed the PD's input power limitation.

In addition, the high RRH-laser output powers ($P_{RRH-laser}$) deliver two extra unique advantages: i) relaxing the requirements of the high RRH-received optical signal powers and thus allowing relatively low optical powers launched into the BBU-RRH fiber links, as verified by Fig. 5. This is beneficial to mitigate the fiber nonlinearity effects and further enhance the network's adaptability to the WDM application scenarios, and ii) reducing the required RoPs for producing the mmWave signals capable of delivering a specific transmission performance or desirable network coverage, as verified by Section IV.D.

Moreover, the results in Fig. 5(b) indicate that expensive EDFAs may be excluded for some application scenarios where the RRH-received optical signals have sufficiently high powers. For the considered experimental setups used in obtaining Fig. 5(b), the minimum CO-BBU launch power corresponding to BERs at the considered FEC limit is ~1.5 dBm. Because the corresponding optical link power losses are ~10 dB (~2 dB due to the fiber transmissions and ~8 dB due to the Soft-ROADM MZM), it is easy to understand that if the CO-BBU uses conventional optical transmitters with a typical ~5 dBm optical launch power, the proposed network without using any optical amplifiers can achieve an optical link power budget of at least 13.5 dB (=5-1.5+10). It should be noted that the RoPs in Fig. 5(b) present the total optical powers launched into the PIN, which contain both the RRH-received optical signal power and the RRH-laser power, as such they cannot be used for calculating the power budget. It is also worth mentioning that the estimated 13.5 dB optical link power budget can be further enhanced by using various techniques, including for example: i) advanced DSP techniques (such as advanced equalization techniques [52]), ii) advanced optical/electrical components (such as avalanche photodiodes (APDs) for producing mmWave signals [38, 40]), and iii) advanced radio

communication techniques (such as multiple-input and multiple-output (MIMO) techniques [12].

Of course, more advanced Soft-ROADM designs that can introduce negligible optical link power losses are highly desirable for considerably improving the optical link power budget. This would be achievable if novel small-footprint, high-bandwidth, and cost-effective Soft-ROADM drop elements are developed by monolithically integrating electro-absorption modulators (EAMs) or MZMs with semiconductor optical amplifiers (SOAs) [53, 54]. Such Soft-ROADMs may also be beneficial in reducing the overall expenditure of the proposed networks.

D. Adaptive mmWave Wireless Coverage

The proposed network offers dynamic and flexible mmWave signal power adjustments by altering the RRH-received optical signal power and/or RRH-laser output power, as demonstrated in Section IV.C. Such mmWave signal power adjustments further give rise to the highly desirable adaptive wireless network coverage.

The experimental setup in Section III is used to evaluate wireless network coverage adaptability and maximum achievable wireless network coverage. For different RRH-received/embedded optical signal/laser powers, the resulting RoPs and the achievable OFDM band-2 performances are given in Fig. 6. The fiber length is fixed at 10 km, and the mmWave frequency is 38 GHz. Various mmWave wireless distances are considered. The RRH-received optical signal power is altered by adjusting the EDFA gain. In obtaining this figure, physical wireless links are used for distances <20 m. For each considered physical mmWave link length, VEA-2 is adaptively adjusted to achieve optimum BER performances in the UE. For wireless link lengths of >20 m, due to the indoor laboratory space limitation, a 20 m actual wireless link plus an emulated wireless link is considered. The emulated link is introduced by adjusting the attenuation of the UE-embedded VEA-2 to offer an extra
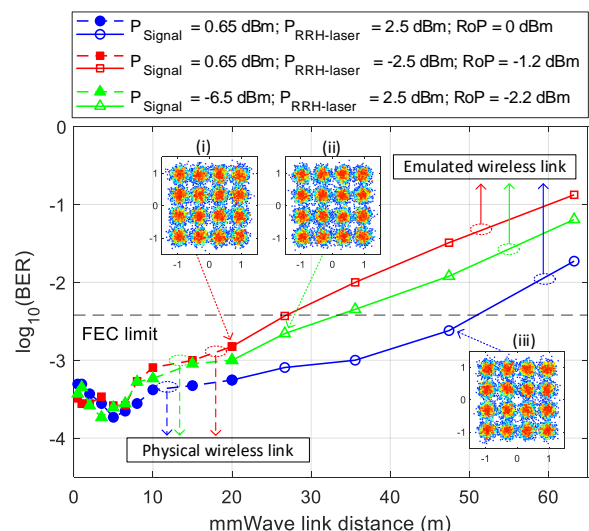

Fig. 6. OFDM band-2 BER performance for different mmWave wireless link lengths. Dashed traces (link distances ≤ 20 m): actual mmWave wireless links. Solid traces (link distances > 20 m): a 20 m actual mmWave wireless link plus an emulated mmWave wireless link.

link power loss, based on the equivalent free-space path loss (FSPL) estimation [55].

As seen in Fig. 6, either increasing the RRH-laser power or increasing the RRH-received optical signal power can lead to relatively high RoPs, thus resulting in relatively high mmWave signal powers and mmWave wireless coverage extension. This agrees with the results in Section IV.C. The results in Fig. 6 indicate that the proposed network can potentially achieve >50 m mmWave wireless coverages. On the other hand, considering a fixed RRH-received optical signal power of 0.65 dBm (P_{Signal}), a 5 dB increase in RRH-embedded laser output power (or a 1.2 dB increase in RoPs) results in an extended wireless coverage range of 24 meters.

It is worth mentioning that the RoP = -2.2 dBm case achieves better BER performances than the RoP = -1.2 dBm case. This is because, for the former case, the EDFA gain is relatively low, thus leading to a relatively high OSNR for the RRH-received optical signals. This implies that for practically extending mmWave network coverages or improving transmission performances, in comparison with increasing the RRH-received optical signal powers, increasing RRH-laser output power is beneficial for achieving better transmission performances. More importantly, it also relaxes the stringent requirements of using high-gain optical amplifiers and high RoPs. The results further validate the statement in Section IV.C, that for altering the produced mmWave signal powers, altering RRH-laser output power is more efficient than varying RRH-received optical signal power via adjusting optical amplifier gains.

The proposed fiber-wireless converged access network potentially possesses theoretically unlimited scalability, because the network has the following features: i) inherent adaptability to wavelength count variations. As one of the network's advantages, as discussed in Section IV.C, high RRH-laser output powers can also be employed to reduce the BBU launch power of each wavelength to support more wavelengths, and ii) capability of providing the "just-the-right-size" sub-wavelength-level BBU-RRH connections: For the proposed network, for each wavelength, the adopted optical transceivers can flexibly adjust the bandwidth of each band by altering its digital filter bandwidth over a bandwidth variation range as large as the sampling speed of the adopted ADC/DAC, as verified in our experimental demonstrations [56]. As the Soft-ROADM sub-wavelength add/drop operation is transparent to signal bandwidth [33, 34, 35], the proposed network can, therefore, convey a theoretically unlimited number of signal bands on a single wavelength. On the other hand, multiple RRHs can share the same signal band through traditional multiplexing techniques such as TDM for further improving the network scalability. Based on the above statements, the proposed network has the potential of providing a highly dynamic and adaptive solution for NG-RANs capable of accommodating a large number of RRHs and/or BBUs.

For the proposed network, the use of Soft-ROADMs and free-running laser-(electrical ED)-enabled mmWave signal generation (detection) not only lowers the overall system latency but also reduces the system complexity, because the following four reasons: i) for the sub-wavelength-level Soft-ROADM drop operation, each UE only receives a targeted signal at the baseband frequency region (after the envelope detector), this allows the use of a low-speed ADC that just operates at a bandwidth of the targeted signal, thus avoiding the need of supporting the whole aggregated BBU signal bandwidth [35], ii) UEs can use conventional signal demodulation DSP procedures without complicated DSP techniques for mitigating phase noise and frequency fluctuation assoicated with the free-running laser-based mmWave signal generation, iii) the proposed network enables data signals to continuously flow between BBUs and UEs without O-E-O conversions or DSP at any intermediate nodes, iv) the adopted BBU transmitters can adopt the real-time parallel digital filter field-programmable gate array (FPGA) designs for aggregating multiple independent signal bands, allowing considerable reductions in DSP complexity and ultra-low latency [57].

V. CONCLUSION

This paper has proposed and experimentally demonstrated a cost-effective fiber-wireless converged dynamic and flexible IM-DD access network capable of simultaneously establishing on-demand connections between the BBU and different UEs without O-E-O conversions and/or extensive DSP at the intermediate nodes. The O-E-O conversion-free Soft-ROADMs are used to provide "just-the-right-size" wavelength/sub-wavelength-level optical switching between the BBU and the RRHs. Free-running laser-(electrical ED)-enabled mmWave signal generation (detection) is utilized to achieve mmWave frequency tunability and adaptive wireless coverage.

The optimum network configuration, the achievable performance, and the aforementioned features of the proposed network have been experimentally explored in a fiber-wireless converged network with 3×1.333 Gbps flexible BBU-UE connections established over a 10 km IM-DD SSMF and a 38 GHz, 5 m mmWave wireless links. The results indicate that appropriately adjusting the RRH-laser output power and its corresponding frequency can adapt mmWave network coverages and tune the mmWave frequency within a wide range, respectively, this is more effective than adjusting the powers of the RRH-received optical signals from the BBU. A relatively high RRH-laser output power may also contribute to reductions in overall network expenditure and power consumption.

REFERENCES

[1] GSMA, "The Mobile Economy 2024," 2024.
[2] W. Jiang, B. Han, M. A. Habibi and H. D. Schotten, "The Road Towards 6G: A Comprehensive Survey," *IEEE Open Journal of the Communications Society,* vol. 2, pp. 334-366, 2021.

[3] Z. Zhang, Y. Xiao, Z. Ma, M. Xao, Z. Ding, X. Lei, G. K. Karagiannidis and P. Fan, "6G Wireless Networks: Vision, Requirements, Architecture, and Key Technologies," *IEEE Vehicular Technology Magazine,* vol. 14, no. 3, pp. 28-41, 20219.

[4] H. Rodrigues Dias Filgueiras, E. Saia Lima, M. Seda Borsato Cunha, C. H. De Souza Lopes, L. Carneiro de Souza, M. B. Ramon, L. A. Melo Pereira, T. H. Brandao, T. P. Villena Andrade, L. Camilo Alexandre, G. Neto, A. Linhares, L. Leonel Mendes, M. Araujo Romero and A. Cerqueira S., "Wireless and Optical Convergent Access Technologies Toward 6G," *IEEE Access,* vol. 11, pp. 9232-9259, 2023.

[5] "5G; NR; User Equipment (UE) radio transmission and reception; Part 1: Range 1 Standalone (ETSI TS 138 101-1 V17.12.0)," 3rd Generation Partnership Project, 2024.

[6] "5G; NR; User Equipment (UE) radio transmission and reception; Part 2: Range 2 Standalone (ETSI TS 138 101-2 V18.5.0)," 3rd Generation Partnership Project, 2024.

[7] X. Wang, L. Kong, F. Kong, F. Qiu, M. Xia, S. Arnon and G. Chen, "Millimeter Wave Communication: A Comprehensive Survey," *IEEE Communications Surveys & Tutorials,* vol. 20, no. 3, pp. 1616-1653, 2018.

[8] M. Sung, S. Kim, E.-S. Kim, S.-R. Moon, M. Kim, I.-M. Lee, K. H. Park, J. K. Lee and S.-H. Cho, "Photonic THz Communications Based on Radio-Over-Fiber Technology for 6G Mobile Network: Design and Opportunity," *IEEE Journal of Selected Topics in Quantum Electronics,* vol. 29, no. 5, 2023.

[9] Jianping Yao, "Microwave Photonics," *Journal of Lightwave Technology,* vol. 27, no. 3, pp. 314-335, 2009.

[10] A. B. Dar and F. Ahmad, "Optical millimeter-wave generation techniques: An overview," *Optik,* vol. 258, 2022.

[11] A. Delmade, C. Browning, T. Verolet, J. Poette, A. Farhang, H. H. Elwan, R. D. Koilpillai, G. Aubin, F. Lelarge, A. Ramdane, D. Venkitesh and L. P. Barry, "Optical Heterodyne Analog Radio-Over-Fiber Link for Millimeter-Wave Wireless Systems," *Journal of Lightwave Technology,* vol. 39, no. 2, pp. 465-474, 2021.

[12] X. Li, J. Yu and G.-K. Chang, "Photonics-Aided Millimeter-Wave Technologies for Extreme Mobile Broadband Communications in 5G," *Journal of Lightwave Technology,* vol. 38, no. 2, pp. 366-378, 2020.

[13] L. Gonzalez-Guerrero, H. Shams, I. Fatadin, M. J. Fice, M. Naftaly, A. J. Seeds and C. C. Renaud, "Single Sideband Signals for Phase Noise Mitigation in Wireless THz-Over-Fibre Systems," *Journal of Lightwave Technology,* vol. 36, no. 19, pp. 4527-4534, 2018.

[14] L. Goldberg, H. F. Taylor, J. F. Weller and D. M. Bloom, "Microwave signal generation with injection-locked laser diodes," *Electronics Letters,* vol. 19, no. 13, pp. 491-493, 1983.

[15] J. Harrison and A. Mooradian, "Linewidth and offset frequency locking of external cavity GaAlAs lasers," *IEEE Journal of Quantum electronics,* vol. 25, no. 6, pp. 1152-1155, 1989.

[16] A. C. Bordonalli, C. Walton and A. J. Seeds, "High-performance phase locking of wide linewidth semiconductor lasers by combined use of optical injection locking and optical phase-lock loop," *Journal of Lightwave Technology,* vol. 17, no. 2, pp. 328-342, 1999.

[17] T. Nakasyotani, H. Toda, T. Kuri and K. Kitayama, "Wavelength-division-multiplexed Millimeter-waveband radio-on-fiber system using a supercontinuum light source," *Journal of Lightwave Technology,* vol. 24, no. 1, pp. 404-410, 2006.

[18] M. Zhao, W. Zhou, L. Zhao, J. Xiao, X. Li, F. Zhao and J. Yu, "A New Scheme to Generate Multi-Frequency Mm-Wave Signals Based on Cascaded Phase Modulator and I/Q Modulator," *IEEE Photonics Journal,* vol. 11, no. 5, 2019.

[19] H. Zhang, L. Cai, S. Xie, K. Zhang, X. Wu and Z. Dong, "A Novel Radio-Over-Fiber System Based on Carrier Suppressed Frequency Eightfold Millimeter Wave Generation," *IEEE Photonics Journal,* vol. 9, no. 5, 2017.

[20] T. Schneider, D. Hannover and M. Junker, "Investigation of Brillouin scattering in optical fibers for the generation of Millimeter waves," *Journal of Lightwave Technology,* vol. 24, no. 1, pp. 295-304, 2006.

[21] P.-T. Shih, J. J. Chen, C.-T. Lin, W.-J. Jiang, H.-S. Huang and P.-C. Peng, "Optical millimeter-wave signal generation via frequency 12-tupling," *Journal of Lightwave Technology,* vol. 28, no. 1, pp. 71-78, 2010.

[22] L. Gonzalez-Guerrero, M. Ali, R. Guzman, H. Lamela and G. Carpintero, "Photonic Sub-Terahertz IM Links: Comparison Between Double and Single Carrier Modulation," *Journal of Lightwave Technology,* vol. 40, no. 18, pp. 6064-6070, 2022.

[23] C.-T. Tsai, C.-C. Li, C.-H. Lin, C.-T. Lin, S. Chi and G.-R. Lin, "Long-reach 60-GHz MMWoF link with free-running laser diodes beating," *Scientific Reports,* vol. 8, no. 13711, pp. 1-14, 2018.

[24] I. Gonzalez Insua, D. Plettemeier and C. G. Schaffer, "Simple Remote Heterodyne Radio-Over-Fiber System for Gigabit Per Second Wireless Access," *Journal of Lightwave Technology,* vol. 28, no. 16, pp. 2289-2295, 2010.

[25] B. C. Collings, "Advanced ROADM Technologies and Architectures," in *Optical Fiber Communication Conference (OFC),* Los Angeles, California, 2015.

[26] H. Yang, B. Robertson, P. Wilkinson and D. Chu, "Low-Cost CDC ROADM Architecture Based on Stacked Wavelength Selective Switches," *Journal of Optical Communications and Networking,* vol. 9, no. 5, pp. 375-384, 2017.

[27] G. Kalfas, C. Vagionas, A. Antonopoulos, E. Kartsakli, A. Mesodiakaki, S. Papaioannou, P. Maniotis, J. S. Vardakas, C. Verikoukis and N. Pleros, "Next Generation Fiber-Wireless Fronthaul for 5G mmWave Networks," *IEEE Communications Magazine,* vol. 57, no. 3, pp. 138-144, 2019.

[28] T. Chen, J. Yu, A. Minakhmetov, C. Gutterman, M. Sherman, S. Zhu, S. Santaniello, A. Biswas, I. Seskar, G. Zussman and D. Kilper, "A Software-Defined Programmable Testbed for Beyond 5G Optical-Wireless Experimentation at City-Scale," *IEEE Network,* vol. 36, no. 2, pp. 90-99, March/April 2022.

[29] C. Browning, Q. Cheng, N. C. Abrams, M. Ruffini, L. Y. Dai, L. P. Barry and K. Bergman, "A Silicon Photonic Switching Platform for Flexible Converged Centralized-Radio Access Networking," *Journal of Lightwave Technology,* vol. 38, no. 19, pp. 5386-, 2020.

[30] C. Vagionas, R. Maximidis, I. Stratakos, A. Margaris, A. Mesodiakaki, M. Gatzianas, K. Kanta, P. Toumasis, G. Giannoulis, D. Apostolopoulos, E. A. Papatheofanous, G. Lentaris, D. Reisis, D. Soudris, K. Tsagkaris, N. Argyris, D. Syrvelis, P. Bakopoulos, R. M. Oldenbeuving, C. G. H. Roeloffzen, P. W. L. van Dijk, I. Dimogiannis, A. Kontogiannis, H. Avramopoulos, A. Miliou, N. Pleros and G. Kalfas, "End-to-End Real-Time Service Provisioning Over a SDN-Controllable Analog mmWave Fiber -Wireless 5G X-Haul Network," *Journal of Lightwave Technology,* vol. 41, no. 4, pp. 1104-1113, 2023.

[31] A. Tsakyridis, E. Ruggeri, G. Kalfas, R. M. Oldenbeuving, P. W. L. van Dijk, C. G. H. Roeloffzen, Y. Leiba, A. Miliou, N. Pleros and C. Vagionas, "Reconfigurable Fiber Wireless IFoF Fronthaul With 60 GHz Phased Array Antenna and Silicon Photonic ROADM for 5G mmWave C-RANs," *IEEE Journal on Selected Areas in Communications,* vol. 39, no. 9, pp. 2816-2826, 2021.

[32] J. Xia, T. Li, Q. Cheng, M. Glick, M. Crisp, K. Bergman and R. Penty, "A Future Proof Reconfigurable Wireless and Fixed Converged Optical Fronthaul Network Using Silicon Photonic Switching Strategies," *Journal of Lightwave Technology,* vol. 41, no. 6, pp. 1610-1618, March 2023.

[33] E. Al-Rawachy, R. P. Giddings and J. M. Tang, "Real-time experimental demonstration of DSP-enabled soft-ROADMs with multi-level flexible add/drop functions for cloud access networks," *Optics Express,* vol. 27, no. 1, pp. 16-33, 2019.

[34] W. Jin, C. Zhang, X. Duan, M. R. Kadhum, Y. X. Dong, R. P. Giddings, N. Jiang, K. Qiu and J. M. Tang, "Improved Performance Robustness of DSP-Enabled Flexible ROADMs Free from Optical Filters and O-E-O Conversions," *Journal of Optical Communications and Networking,* vol. 8, no. 8, pp. 521-529, 2016.

[35] O. F. A. Gonem, R. P. Giddings and J. Tang, "Experimental Demonstration of Soft-ROADMs With Dual-Arm Drop Elements for Future Optical-Wireless Converged Access Networks," *Journal of Lightwave Technology,* vol. 42, no. 6, pp. 1773-1785, 2024.

[36] W. Jin, X. Duan, Y. Dong, B. Cao, R. P. Giddings, C. Zhang, K. Qiu and J. M. Tang, "DSP-Enabled Flexible ROADMs Without Optical Filters and O-E-O Conversions," *Journal of Lightwave Technology,* vol. 33, no. 19, pp. 4124-4131, October 2015.

[37] A. Kanno, P. T. Dat, N. Yamamoto, T. Kawanishi, N. Iwasawa, N. Iwaki, K. Nakamura, K. Kawasaki, N. Kanada, N. Yonemoto, Y. Sato, M. Fujii, K. Yanatori, N. Shibagaki and K. Kashima, "High-Speed Railway Communication System Using Linear-Cell-Based Radio-Over-Fiber Network and Its Field Trial in 90-GHz Bands," *Journal of Lightwave Technology,* vol. 38, no. 1, pp. 112-122, Jan. 2020.

[38] R. Maximidis, C. Vagionas, G. Kalfas, Y. Leiba, A. Miliou and N. Pleros, "A 51 Gb/s Reconfigurable mmWave Fiber-Wireless C-RAN Supporting 5G/6G MNO Network Sharing," *Journal of Lightwave Technology,* vol. 41, no. 14, pp. 4705-4712, Jul. 2023.

[39] P. Toumasis, K. Kanta, C. Vagionas, G. Giannoulis, Z. S. He, G. Torfs, E. Kyriazi, G. Brestas, R. Maximidis, C. Meysmans, W. Wasko, D. Apostolopoulos, A. Miliou, N. Pleros and H. Avramopoulos, "First real-time demonstration of a flexible multi-λ DRoF/ARoF/SDoF transport for fiber/mmWave RAN," in *49th European Conference on Optical Communications (ECOC 2023),* Hybrid Conference, Glasgow, UK, 2023.

[40] K. Zhang, Q. Zhuge, H. Xin, H. He, W. Hu and D. V. Plant, "Low-Cost WDM Fronthaul Enabled by Partitioned Asymmetric AWGR With Simultaneous Flexible Transceiver Assignment and Chirp Management," *Journal of Optical Communications and Networking,* vol. 9, no. 10, pp. 876-888, Oct. 2017.

[41] C. Vagionas, R. Maximidis, I. Stratakos, A. Margaris, A. Mesodiakaki, M. Gatzianas, K. Kanta, P. Toumasis, G. Giannoulis, D. Apostolopoulos, E. A. Papatheofanous, G. Lentaris, D. Reisis, D. Soudris, K. Tsagkaris, N. Argyris, D. Syrivelis, P. Bakopoulos, R. M. Oldenbeuving, C. G. H. Roeloffzen, P. W. L. van Dijk, I. Dimogiannis, A. Kontogiannis, H. Avramopoulos, A. Miliou, N. Pleros and G. Kalfas, "End-to-End Real-Time Service Provisioning over a SDN-controllable 60 GHz analog FiWi X-haul for 5G Hot-Spot Networks," in *2022 Optical Fiber Communications Conference and Exhibition (OFC)*, San Diego, CA, USA, 2022.

[42] E. Ruggeri, C. Vagionas, R. Maximidis, G. Kalfas, D. Spasopoulos, N. Terzenidis, R. M. Oldenbeuving, P. W. L. van Dijk, C. G. H. Roeloffzen, N. Pleros and A. Miliou, "Reconfigurable Fiber Wireless Fronthaul With A-RoF and D-RoF Co-Existence Through a Si3N4 ROADM for Heterogeneous Mmwave 5G C-RANs," *Journal of Lightwave Technology,* vol. 40, no. 16, pp. 5514-5521, Aug. 2022.

[43] A. Tsakyridis, E. Ruggeri, G. Kalfas, R. M. Oldenbeuving, P. W. L. van Dijk, C. Roeloffzen, Y. Leiba, A. Miliou, N. Pleros and C. Vagionas, "A Flexible and Reconfigurable Si3N4 ROADM-enabled 5G mmWave IFoF Fiber Wireless Fronthaul with 60 GHz beamsteering capabilities," in *2020 European Conference on Optical Communications (ECOC)*, Brussels, Belgium, 2020.

[44] D. Dass, L. Y. Dai, K. Bergman, X. Ouyang, P. Townsend, C. Roeloffzen and C. Browning, "Low Noise Ultra-Flexible SiP Switching Platform for mmWave OCDM & Multi-Band OFDM ARoF Fronthaul," *IEEE Photonics Technology Letters,* vol. 35, no. 12, pp. 653-656, Jun. 2023.

[45] M. Bolea, R. P. Giddings, M. Bouich, C. Aupetit-Berthelemot and J. M. Tang, "Digital Filter Multiple Access PONs With DSP-Enabled Software Reconfigurability," *Journal of Optical Communications and Networking,* vol. 7, no. 4, pp. 215-222, 2015.

[46] M. L. Deng, X. Duan, W. Jin, R. P. Giddings, S. Mansoor and J. M. Tang, "Experimental demonstration and performance evaluation of flexible add/drop operations of DSP-switched ROADMs for cloud access networks," *Optics Communications,* vol. 428, pp. 95-103, 2018.

[47] X. Duan, M. L. Deng, W. Jin, R. P. Giddings, S. Mansoor and J. M. Tang, "Experimental Demonstration of DSP-enabled Drop Operations of Flexible ROADMs Excluding Optical Filters and O-E-O Conversions," in *Optical Fiber Communication Conference (OFC)*, Anaheim, California, 2016.

[48] W. Jin, Z. Q. Zhong, S. Jiang, J. X. He, D. Chang, Y. H. Hong, R. P. Giddings, X. Q. Jin, M. O'Sullivan, T. Durrant, J. Trewern, G. Mariani and J. M. Tang, "Rectangular Orthogonal Digital Filter Banks Based on Extended Gaussian Functions," *Journal of Lightwave Technology,* vol. 40, no. 12, pp. 3709-3722, June 2022.

[49] O. F. A. Gonem, R. P. Giddings and J. Tang, "Drop Signal Phase Offset Independent Soft-ROADMs for Point-to-Multipoint 5G Fronthauls," in *2023 Opto-Electronics and Communications Conference (OECC)*, Shanghai, China, 2023.

[50] Y. Zhu, X. Ruan, K. Zou and F. Zhang, "Beyond 200G Direct Detection Transmission With Nyquist Asymmetric Twin-SSB Signal at C-Band," *Journal of Lightwave Technology,* vol. 35, no. 17, pp. 3629-3636, September 2017.

[51] E. Berikaa, M. S. Alam and D. V. Plant, "Beyond 300 Gbps Short-Reach Links Using TFLN MZMs With 500 mVpp and Linear Equalization," *IEEE Photonics Technology Letters,* vol. 35, no. 3, pp. 140-143, February 2023.

[52] A. Sun, Z. Li, J. Jia, B. Dong, S. Xing, G. Li, C. Huang, A. Yan, P. Luo, J. Shi, N. Chi and J. Zhang, "End-to-End Deep-Learning-Based Photonic-Assisted Multi-User Fiber-mmWave Integrated Communication System," *Journal of Lightwave Technology,* vol. 42, no. 1, pp. 80-94, Jan. 2024.

[53] T. Hiraki, T. Aihara, T. Fujii, K. Takeda, T. Kakitsuka, T. Tsuchizawa and S. Matsuo, "Membrane InGaAsP Mach–Zehnder Modulator Integrated With Optical Amplifier on Si Platform," *Journal of Lightwave Technology,* vol. 38, no. 11, pp. 3030-3036, Jun. 2020.

[54] Z. Sun, W. Sun, R. Xiao, J. Zhao, K. Tang, Z. Xu, Y. Ma, W. Wang, Y.-J. Chiu and X. Chen, "Enhanced Performance of Wavelength-tunable EML Based on REC Technique," *Journal of Lightwave Technology,* 2024.

[55] J. G. Proakis and M. Salehi, Digital Communications, McGraw-Hill, 2008.

[56] W. Jin, Z. Q. Zhong, S. Jiang, J. X. He, S. H. Hu, D. Chang, R. P. Giddings, Y. H. Hong, X. Q. Jin, M. O'Sullivan, T. Durrant, J. Trewern, G. Mariani and J. M. Tang, "Experimental demonstrations of DSP-enabled flexibility, adaptability and elasticity of multi-channel >72Gb/s over 25 km IMDD transmission systems," *Optics Express,* vol. 29, no. 25, pp. 41363-41377, Dec. 2021.

[57] E. Al-Rawachy, R. P. Giddings and J. Tang, "Experimental Demonstration of a Real-Time Digital Filter Multiple Access PON With Low Complexity DSP-Based Interference Cancellation," *Journal of Lightwave Technology,* vol. 37, no. 17, pp. 4315-4329, Sep. 2019.